Screened hybrid density functionals applied to solids

Cite as: J. Chem. Phys. **124**, 154709 (2006); https://doi.org/10.1063/1.2187006
Submitted: 17 January 2006 • Accepted: 21 February 2006 • Published Online: 19 April 2006

J. Paier, M. Marsman, K. Hummer, et al.

Screened hybrid density functionals applied to solids

J. Paier,[a] M. Marsman, K. Hummer, and G. Kresse
Institut für Materialphysik, Universität Wien and Center for Computational Material Science, Sensengasse 8, A-1090, Wien, Austria

I. C. Gerber and J. G. Ángyán
Laboratoire de Cristallographie et de Modélisation des Matériaux Minéraux et Biologiques, UMR 7036, Université Henri Poincaré, B. P. 239, F-54506 Vandœuvre-lès-Nancy, France

(Received 17 January 2006; accepted 21 February 2006; published online 19 April 2006)

Hybrid Fock exchange/density functional theory functionals have shown to be very successful in describing a wide range of molecular properties. For periodic systems, however, the long-range nature of the Fock exchange interaction and the resultant large computational requirements present a major drawback. This is especially true for metallic systems, which require a dense Brillouin zone sampling. Recently, a new hybrid functional [HSE03, J. Heyd, G. E. Scuseria, and M. Ernzerhof, J. Chem. Phys. **118**, 8207 (2003)] that addresses this problem within the context of methods that evaluate the Fock exchange in real space was introduced. We discuss the advantages the HSE03 functional brings to methods that rely on a reciprocal space description of the Fock exchange interaction, e.g., all methods that use plane wave basis sets. Furthermore, we present a detailed comparison of the performance of the HSE03 and PBE0 functionals for a set of archetypical solid state systems by calculating lattice parameters, bulk moduli, heats of formation, and band gaps. The results indicate that the hybrid functionals indeed often improve the description of these properties, but in several cases the results are not yet on par with standard gradient corrected functionals. This concerns in particular metallic systems for which the bandwidth and exchange splitting are seriously overestimated. © *2006 American Institute of Physics*. [DOI: 10.1063/1.2187006]

I. INTRODUCTION

In the last decade, density functional theory (DFT) has proven to be a very powerful tool for the quantitative prediction of material properties in the field of solid state physics as well as in chemistry. In its most commonly applied approximation to the electronic exchange and correlation, i.e., in the local density approximation (LDA), DFT has been very successful, perhaps even surprisingly so. Rising to the second rung on so-called Jacob's ladder of the exchange-correlation density functionals[1]—the addition of nonempirical generalized gradient corrections[2] (GGAs)—significantly improves most of the main drawbacks of the LDA; this is especially true for molecular binding energies, and also for some aspects of the description of the structural properties of solids. As a next step, the introduction of so-called hybrid functionals,[3,4] such as PBE0 and B3LYP, obtained by admixing a fixed amount of the Fock exchange, presents a significant improvement over the GGA description of molecular properties. Until recently, however, the large computational effort required to evaluate the Fock exchange under periodic boundary conditions made the application of these hybrid schemes to periodic systems almost intractable and only a few systematic studies were undertaken using the B3LYP functional:[3] e.g., prediction of band gaps[5] and comparative study of structural properties of isostructural oxides.[6]

In a real space formalism, most of the difficulties in evaluating the Fock exchange arise from the slow decay of the exchange interaction with distance. A new hybrid functional, recently proposed by Heyd *et al.* (HSE03),[7] addresses this problem by separating the description of the exchange interaction into a short- and a long-range part. The mix of Fock and DFT exchange is then made only in the short-range part, leaving the long-range exchange interactions to be represented solely by the corresponding part of the range-separated DFT functional. The HSE03 functional yields a description of molecular properties comparable to the results obtained using the PBE0 functional and in some cases it even gives a slight improvement over the latter (see Ref. 7). Heyd and Scuseria[8] made also an assessment of the HSE03 functional for several solid state systems using Gaussian-type orbitals (GTOs). Their results are in good agreement with experiment for various properties such as lattice constants, bulk moduli, and band gaps.[9] Although slightly less so for metallic systems, the results obtained for semiconducting and ionic systems show the HSE03 functional to be superior to the usual density functionals, such as LDA, PBE, and TPSS meta-GGA.[10] A comparison, however, between the performance of the PBE0 and HSE03 functionals, applied to solid state systems, has not been made so far. The recent addition of Fock exchange and hybrid functionals[11] to the features included in the VASP code[12,13] allowed for the implementation of the HSE03 functional with relative ease.

In a real space formalism, the computational advantage of the HSE03 functional over the PBE0 functional stems from the elimination of the long-range part of the Fock exchange, which leads to a reduction of the domain over which the real space integrals have to be evaluated. When the Fock

[a]Electronic mail: joachim.paier@univie.ac.at

exchange operator is evaluated in reciprocal space,[14] as it is the most efficient within a plane wave formalism, the reduction in the computational requirement associated with the HSE03 scheme is expected to be of a different kind: within a band structure picture, the increased locality of the HSE03 Fock exchange interactions allows us to evaluate the short-range Fock operator on a coarser k mesh than would be needed to accurately capture the features of the full Fock exchange operator. Since the computational cost of evaluating the Fock exchange scales quadratically with the number of k points, the reduction in the computational workload connected to the use of the HSE03 functional can be considerable.

In this work we will present a detailed evaluation of the description of solid state properties using the PBE0 and HSE03 functionals within the framework of the plane wave projector augmented wave (PAW) formalism. To this end we will present calculations on several structural (lattice parameters, bulk moduli, and cohesive energies) and electronic (band gaps, bandwidth) properties for a selection of archetypical metallic, semiconducting, and ionic solid state systems. Although there remains some caveats that need to be considered in the future, our main conclusion is that hybrid functionals work remarkably well for systems with intermediate gaps and their computational requirements can be kept at a reasonable level by the use of a screened Fock exchange operator.

II. THEORETICAL BACKGROUNDS

A. The PBE0 and HSE03 functionals

The "parameter-free" PBE0 hybrid functional[4,15] offers many attractive features. It is constructed by a rational mixing of 25% Fock exchange with 75% of the well-known PBE exchange.[16] We note, however, that it has been argued that the ratio of the required nonlocal exchange is system dependent (see Refs. 4 and 17). The electron correlation is represented by the correlation part of the PBE density functional.[16] The resulting expression for the exchange-correlation energy then takes the following simple form:

$$E_{xc}^{\mathrm{PBE0}} = \tfrac{1}{4}E_x + \tfrac{3}{4}E_x^{\mathrm{PBE}} + E_c^{\mathrm{PBE}}, \tag{1}$$

where the nonlocal Fock exchange energy E_x (in real space) can be written as

$$E_x = -\frac{e^2}{2}\sum_{\mathbf{k}n,\mathbf{q}m} 2w_{\mathbf{k}}f_{\mathbf{k}n}\times 2w_{\mathbf{q}}f_{\mathbf{q}m} \times \int\int d^3\mathbf{r}d^3\mathbf{r}'\frac{\phi_{\mathbf{k}n}^*(\mathbf{r})\phi_{\mathbf{q}m}(\mathbf{r})\phi_{\mathbf{q}m}^*(\mathbf{r}')\phi_{\mathbf{k}n}(\mathbf{r}')}{|\mathbf{r}-\mathbf{r}'|} \tag{2}$$

in terms of the set of one-electron Bloch states $\{\phi_{\mathbf{k}n}(\mathbf{r})\}$ of the system and the corresponding set of (possibly fractional) occupational numbers $\{f_{\mathbf{k}n}\}$. The sums over $\mathbf{k}$ and $\mathbf{q}$ need to be performed over all k points chosen to sample the Brillouin zone (BZ), whereas the sums over m and n are performed over all bands at these k points. The k-point weights $w_{\mathbf{k}}$ sum to one and the factors 2 account for the fact that we consider a closed-shell system with doubly occupied one-electron states.

The corresponding nonlocal Fock exchange potential is given by

$$V_x(\mathbf{r},\mathbf{r}') = -e^2\sum_{\mathbf{q}m} 2w_{\mathbf{q}}f_{\mathbf{q}m}\frac{\phi_{\mathbf{q}m}^*(\mathbf{r}')\phi_{\mathbf{q}m}(\mathbf{r})}{|\mathbf{r}-\mathbf{r}'|} = -e^2\sum_{\mathbf{q}m} 2w_{\mathbf{q}}f_{\mathbf{q}m}e^{-i\mathbf{q}\cdot\mathbf{r}'}\frac{u_{\mathbf{q}m}^*(\mathbf{r}')u_{\mathbf{q}m}(\mathbf{r})}{|\mathbf{r}-\mathbf{r}'|}e^{i\mathbf{q}\cdot\mathbf{r}}, \tag{3}$$

where $u_{\mathbf{q}m}(\mathbf{r})$ is the cell periodic part of the Bloch state, $\phi_{\mathbf{q}m}(\mathbf{r})$, at k point $\mathbf{q}$ with band index m.

Using the decomposition of the Bloch states, $\phi_{\mathbf{q}m}$, in plane waves,

$$\phi_{\mathbf{q}m}(\mathbf{r}) = \frac{1}{\sqrt{\Omega}}\sum_{\mathbf{G}} C_{\mathbf{q}m}(\mathbf{G})e^{i(\mathbf{q}+\mathbf{G})\cdot\mathbf{r}}, \tag{4}$$

Eq. (3) can be rewritten as

$$V_x(\mathbf{r},\mathbf{r}') = \sum_{\mathbf{k}}\sum_{\mathbf{G}\mathbf{G}'} e^{i(\mathbf{k}+\mathbf{G})\cdot\mathbf{r}}V_{\mathbf{k}}(\mathbf{G},\mathbf{G}')e^{-i(\mathbf{k}+\mathbf{G}')\cdot\mathbf{r}'}, \tag{5}$$

where

$$V_{\mathbf{k}}(\mathbf{G},\mathbf{G}') = \langle\mathbf{k}+\mathbf{G}|\hat{V}_x|\mathbf{k}+\mathbf{G}'\rangle = -\frac{4\pi e^2}{\Omega}\sum_{m\mathbf{q}} 2w_{\mathbf{q}}f_{\mathbf{q}m} \times\sum_{\mathbf{G}''}\frac{C_{\mathbf{q}m}^*(\mathbf{G}'-\mathbf{G}'')C_{\mathbf{q}m}(\mathbf{G}-\mathbf{G}'')}{|\mathbf{k}-\mathbf{q}+\mathbf{G}''|^2} \tag{6}$$

is the representation of the Fock exchange potential in reciprocal space.[14] The present implementation relies on fast Fourier transforms to avoid convolutions, as explained in Ref. 11.

The description of finite systems using the PBE0 functional has been widely studied.[15,18] The significant improvement with respect to the PBE calculations can be attributed to the fact that the use of a fixed portion of the Fock exchange reduces the self-interaction error of the density functional.[19] Under periodic boundary conditions, i.e., for infinite systems, its application within a real space formalism (employing, for instance, a Gaussian basis set) is still prohibitive, because of the slow convergence of the exchange interaction with distance. To avoid the calculation of the expensive integrals over the slowly decaying long-ranged part of the Fock exchange, Heyd *et al.*[7] proposed to replace it by the corresponding density functional counterpart. The resulting expression for the exchange-correlation energy (HSE03) is given by

$$E_{xc}^{\mathrm{HSE03}} = \tfrac{1}{4}E_x^{\mathrm{sr},\mu} + \tfrac{3}{4}E_x^{\mathrm{PBE,sr},\mu} + E_x^{\mathrm{PBE,lr},\mu} + E_c^{\mathrm{PBE}}. \tag{7}$$

As can be seen from Eq. (7), only the exchange component of the electron-electron interaction is separated into a short- (sr) and a long-range (lr) part. The complete electronic correlation is represented by the standard correlation part of the PBE density functional.

A simple decomposition of the Coulomb kernel[20–23] can be obtained using the construction

$$\frac{1}{r} = S_\mu(r) + L_\mu(r) = \frac{\mathrm{erfc}(\mu r)}{r} + \frac{\mathrm{erf}(\mu r)}{r}, \tag{8}$$

where $r=|\mathbf{r}-\mathbf{r}'|$ and μ is the parameter that defines the range separation related to a characteristic distance $(2/\mu)$ at which the short-range interactions become negligible. In the context of the HSE03 functional, it has been empirically established that the optimum range-separation parameter, μ, is approximately 0.3 Å^{-1}.[7] Using the decomposed Coulomb kernel [Eq. (8)] and Eq. (2), one obtains straightforwardly

$$E_x^{\mathrm{sr},\mu} = -\frac{e^2}{2}\sum_{\mathbf{k}n,\mathbf{q}m} 2w_{\mathbf{k}} f_{\mathbf{k}n} 2w_{\mathbf{q}} f_{\mathbf{q}m} \times \int\int d^3\mathbf{r} d^3\mathbf{r}' \frac{\mathrm{erfc}(\mu|\mathbf{r}-\mathbf{r}'|)}{|\mathbf{r}-\mathbf{r}'|} \times \phi^*_{\mathbf{k}n}(\mathbf{r})\phi_{\mathbf{q}m}(\mathbf{r})\phi^*_{\mathbf{q}m}(\mathbf{r}')\phi_{\mathbf{k}n}(\mathbf{r}'). \tag{9}$$

The representation of the corresponding short-range Fock exchange potential in reciprocal space is given by

$$V_{\mathbf{k}}^{\mathrm{sr},\mu}(\mathbf{G},\mathbf{G}') = \langle \mathbf{k}+\mathbf{G}|\hat{V}_x^{\mathrm{sr},\mu}|\mathbf{k}+\mathbf{G}'\rangle = -\frac{4\pi e^2}{\Omega}\sum_{m\mathbf{q}} 2w_{\mathbf{q}} f_{\mathbf{q}m} \times \sum_{\mathbf{G}''} \frac{C^*_{\mathbf{q}m}(\mathbf{G}'-\mathbf{G}'')C_{\mathbf{q}m}(\mathbf{G}-\mathbf{G}'')}{|\mathbf{k}-\mathbf{q}+\mathbf{G}''|^2} \times (1-e^{-|\mathbf{k}-\mathbf{q}+\mathbf{G}''|^2/4\mu^2}). \tag{10}$$

The only difference to the reciprocal space representation of the complete (undecomposed) Fock exchange potential, given by Eq. (6), is the second factor in the summand in Eq. (10), representing the complementary error function in reciprocal space. Note that Eq. (10) shows the range-separated exchange interaction to belong to the class of screened exchange interactions, for which the representation of the Coulomb kernel in reciprocal space is of the general form

$$\frac{4\pi e^2}{|\mathbf{G}|^2}\cdot \epsilon^{-1}(|\mathbf{G}|), \tag{11}$$

where $\epsilon(|\mathbf{G}|)\sim(1-\mathrm{e}^{-|\mathbf{G}|^2/4\mu^2})^{-1}$ defines the screening of the electrostatic interactions. Obviously, the PBE0 Fock exchange belongs to this family of screened exchange interactions as well [$\epsilon(|\mathbf{G}|)=4$].

The short-range PBE exchange energy and potential, as well as their long-range counterparts, are arrived at using the same decomposition [Eq. (8)], in accordance with Heyd *et al.*[7] It is easily seen from Eq. (8) that the long-range term becomes zero for $\mu=0$ and the short-range contribution then equals the full Coulomb operator, whereas for $\mu\to\infty$ it is the other way around. Consequently, the two limiting cases of the HSE03 functional [see Eq. (7)] are the PBE0 functional for $\mu=0$ and a pure PBE calculation for $\mu\to\infty$.

B. Downsampling E_x^{sr} in reciprocal space

Consider the description of a bulk system, using a supercell made up of N primitive cells, in such a way that the lattice vectors of the supercell are given by $\mathbf{a}'_i = n_i\mathbf{a}_i$ $(i=1,2,3)$, where $\mathbf{a}_i$ are the lattice vectors of the primitive cell. Let $R_{\max}$ be the distance for which

$$\frac{\mathrm{erfc}(\mu|\mathbf{r}-\mathbf{r}'|)}{|\mathbf{r}-\mathbf{r}'|} \approx 0 \quad \text{for } |\mathbf{r}-\mathbf{r}'| > R_{\max}. \tag{12}$$

When the nearest-neighbor distance between the periodically repeated images of the supercell $R_{\mathrm{NN}}>2R_{\max}$, the short-range Fock exchange potential, $V_x^{\mathrm{sr},\mu}$, can be represented exactly, sampling the BZ at the Γ point only, i.e.,

$$V_x^{\mathrm{sr},\mu}(\mathbf{r},\mathbf{r}') = -e^2\sum_m 2f_{\Gamma m}u^*_{\Gamma m}(\mathbf{r}')u_{\Gamma m}(\mathbf{r})\frac{\mathrm{erfc}(\mu|\mathbf{r}-\mathbf{r}'|)}{|\mathbf{r}-\mathbf{r}'|}. \tag{13}$$

This is equivalent to a representation of the bulk system using the primitive cell and a $(n_1\times n_2\times n_3)$ sampling of the BZ,

$$V_x^{\mathrm{sr},\mu}(\mathbf{r},\mathbf{r}') = -e^2\sum_{\mathbf{q}m'} 2w_{\mathbf{q}} f_{\mathbf{q}m'} e^{-i\mathbf{q}\cdot\mathbf{r}'} u^*_{\mathbf{q}m'}(\mathbf{r}')u_{\mathbf{q}m'}(\mathbf{r})e^{i\mathbf{q}\cdot\mathbf{r}} \times \frac{\mathrm{erfc}(\mu|\mathbf{r}-\mathbf{r}'|)}{|\mathbf{r}-\mathbf{r}'|}, \tag{14}$$

where the set of $\mathbf{q}$ vectors is given by

$$\{\mathbf{q}\} = \left\{ \frac{m_1}{n_1}\mathbf{b}_1 + \frac{m_2}{n_2}\mathbf{b}_2 + \frac{m_3}{n_3}\mathbf{b}_3 | m_i = 0,\ldots,n_i-1 \right\}, \tag{15}$$

and $\mathbf{b}_{1,2,3}$ are the reciprocal lattice vectors of the primitive cell.

In light of the above, it is clear that the number of q points needed to represent the short-range Fock exchange potential decreases with decreasing $R_{\max}$ and increasing μ, respectively. Furthermore, one should realize that the maximal range of the exchange interactions is not only governed by the complementary error function $\mathrm{erfc}(\mu|\mathbf{r}-\mathbf{r}'|)/|\mathbf{r}-\mathbf{r}'|$ but also depends on the extent of the spatial overlap of the one-electron states. For the Fock exchange energy, this can be easily shown by adopting a Wannier representation of the one-electron wave functions in Eq. (2) or (9). The radius $R_{\max}$, as defined in Eq. (12), therefore, provides an upper limit for the range of the exchange interactions, consistent with slowly decaying Wannier functions (metals).

Thus, in most cases, the short-range Fock potential may be represented on a considerably coarser mesh of points in the BZ than other contributions to the Hamiltonian. To take advantage of this situation, we restrict the sum over $\mathbf{q}$ in Eq. (10) to a subset, $\{\mathbf{q}\}_{\mathbf{k}}$, of the full $(N_1\times N_2\times N_3)$ k-point set $\{\mathbf{k}\}$, for which the following holds:

$$\{\mathbf{q}\}_{\mathbf{k}} = \left\{ \mathbf{k} + \sum_{i=1}^{3}\frac{m_i C_i}{N_i}\mathbf{b}_i | m_i = 0,\ldots,\frac{N_i}{C_i}-1 \right\}, \tag{16}$$

where C_i is an integer "grid-reduction factor" along the reciprocal lattice direction $\mathbf{b}_i$. Note that the q-point grids are centered at the k point $\mathbf{k}$ at which $V_{\mathbf{k}}(\mathbf{G},\mathbf{G}')$ needs to be evaluated. This is required to allow for a proper treatment of the long-range singularities in the Coulomb potential if the

TABLE I. Parameters of the PAW data sets used in the present work. In all cases, two partial waves are used for the *s* and *p* orbitals. "valence" indicates which orbitals are treated as valence orbitals; r_c^l are the cutoff radii for the partial waves. If small indices are used, they indicate which cutoff was used for *s*-, *p*-, and *d*-partial waves. E_{cut} are the energy cutoffs for which $\Delta E_{\mathrm{kin}} < 0.1$ mRy.

	Valence	r_c^l(a.u.)	E_{cut} (eV)
Li	$1s2s2p$	1.7	500
B	$2s2p1$	1.5_s,1.7_p	320
C	$2s2p$	1.2_s,1.5_p	400
N	$2s2p$	1.2_s,1.5_p	400
O	$2s2p$	1.2_s,1.52_p	400
F	$2s2p$	1.2_s,1.52_p	400
Na	$2p3s$	2.2	260
Mg	$3s3p$	2.0	270
Al	$3s3p$	1.9	245
Si	$3s3p$	1.9	250
P	$3s3p$	1.9	270
Cl	$3s3p$	1.9	280
Cu	$3d4s$	2.3	295
Ga	$3d4s4p$	2.3	285
As	$4s4p$	2.1	210
Rh	$4p4d5s5p$	2.1_p,$2.4_{s,d}$	250
Pd	$4p4d5s5p$	2.1_p,$2.4_{s,d}$	255
Ag	$4d5s$	$2.4_{s,d}$	250

bare Fock operator is used.[11] The outlined procedure reduces the computational workload by a factor of $C_1C_2C_3$.

III. COMPUTATIONAL SETUP

A. PAW calculations

The calculations presented in this work were performed with an (as yet) unreleased version of the Vienna *ab initio* simulation package (VASP),[13] which includes an implementation of the Fock exchange operator[11] and the closely related PBE0 and HSE03 hybrid functionals. To describe the electron-ion interactions, VASP employs the full-potential PAW method.[24,25] The range-separated exchange integrals of the HSE03 functional were calculated on the radial augmentation grid, according to the usual PAW algorithm, using the recently derived spherical harmonic expression of the short-range interaction kernel.[26]

The parameters of the PAW data sets used in the present work are summarized in Table I. The cutoff energies E_{cut}, listed in Table I, are sufficient to reduce the kinetic-energy errors for atomic one-electron wave functions (ΔE_{kin}) to 0.1 mRy (see Ref. 27). To minimize errors arising from the frozen core approximation, we used PAW data sets treating the Rh and Pd 4*p* states, the Ga 3*d* states, and the Li 1*s* states as valence electrons.

In order to compare the accuracy of our implementation of the HSE03 functional with the results of Heyd and Scuseria[8] we performed our calculations on the same selection of bulk systems as that of these authors.

The theoretical lattice constants and bulk moduli were determined by fitting the volume dependence of the static lattice energy [weighted seven point fit; covering an interval of roughly $(0.9,1.1)\Omega_{\mathrm{exp}}$, where Ω_{exp} is the experimental equilibrium volume] to a Murnaghan equation of state.[28] In order to reduce the effects of changes in the size of the basis set due to changes in the unit cell volume, all calculations were performed at an energy cutoff roughly 30% larger than the relevant value listed in Table I.

TABLE II. Combinations of "full" ({**k**}) and "downsampled" ({**q**}) meshes used to evaluate the effect of downsampling the reciprocal space representation of the Fock exchange operator in the PBE0 and HSE03 functionals.

{**k**}	{**q**}		$(n_1\times n_2\times n_3)$	
$(N_1\times N_2\times N_3)$				
$24\times24\times24$	$12\times12\times12$	$8\times8\times8$	$6\times6\times6$	$4\times4\times4$
$16\times16\times16$	$8\times8\times8$	$4\times4\times4$		
$12\times12\times12$	$6\times6\times6$	$4\times4\times4$	$3\times3\times3$	
$8\times8\times8$	$4\times4\times4$	$2\times2\times2$		

All Brillouin zone integrations were performed on Γ-centered symmetry reduced Monkhorst-Pack[29] meshes using the tetrahedron method with Blöchl corrections.[30] To facilitate a direct comparison to the work of Heyd and Scuseria[8] the PBE calculations were carried out using $(24\times24\times24)$ *k*-point meshes. Since such a dense sampling of the BZ would be extremely expensive in the case of PBE0 and HSE03 calculations, we investigated to which degree the *k*-point grids can be reduced without sacrificing the accuracy. For the PBE functional, $(12\times12\times12)$ *k* points give *identical values for the lattice constant and bulk modulus to within all specified digits*. Note that the quadratic corrections in the tetrahedron method usually yield very fast convergence with respect to the sampling density in the BZ.[30] While the quoted PBE values can be considered as fully converged with respect to the *k* grids, it is not certain that the same applies to the hybrid functionals. In the latter case, one can vary the Brillouin zone sampling (*k* grid) and/or use a coarser grid for the representation of the (short-range) Fock exchange operator. To distinguish these two meshes we will refer to the possibly coarser mesh applied in the Fock exchange operator as *q* grid.

The effects of downsampling the reciprocal space representation of the Fock exchange operator in the PBE0 and HSE03 functionals were investigated for a series of different combinations of "full" *k*-point meshes, on which all contributions to the Hamiltonian except the Fock exchange are represented and their corresponding "downsampled" subsets of *q* points, on which only the Fock exchange is evaluated (see Sec. II B). These combinations are listed in Table II and we will from now on refer to these meshes using the notation $(N_1\times N_2\times N_3)/(n_1\times n_2\times n_3)$. This strategy allows us to determine both the minimal *k*-mesh sampling needed to converge the total energy as well as the downsampled *q* mesh sufficient to converge the calculation of the Fock exchange contributions. Note that a coarser grid for the Fock exchange offers the greatest advantages for metallic systems, which require many *k* points to yield converged energies.

As will be shown in Sec. IV A, HSE03 calculations are well converged using $(12\times12\times12)/(6\times6\times6)$ *k* points. In the interest of reducing the computational requirements, all HSE03 calculations of equilibrium volumes, bulk moduli, and gaps were initially performed on this combination of

TABLE III. Input parameters for WIEN2K calculations: the semicore and valence orbitals together with the plane wave cutoff $R_{MT}K_{max}$ and the atomic sphere radii R_{MT} are listed. Note that K_{max}^2 corresponds to the energy cutoff in the PAW calculations. In the case of the compounds MgO and GaAs, the R_{MT} is equal for both elements.

Solid	Valence	R_{MT}(a.u.)	$R_{MT}K_{max}$
Li	$1s2s2p$	1.70	7.5
Na	$2s2p3s3p$	2.50	7.0
Al	$2p3s3p$	2.20	10.0
C	$2s2p$	1.08	7.0
MgO	$2s2p3s3p/2s2p$	1.80	8.0
GaAs	$3d4s4p$	2.20	10.0
Cu	$3p3d4s$	1.90	10.0
Rh	$4p4d5s$	2.20	10.0
Pd	$4p4d5s$	2.40	10.0
Ag	$4p4d5s$	2.60	10.0

grids. For the metallic systems and C, Si, and MgO, the HSE03 calculations were additionally carried out using $(24\times24\times24)/(8\times8\times8)$ meshes. For the remaining systems a $(12\times12\times12)/(12\times12\times12)$ mesh was utilized as reported in Tables VI and VII. As for the PBE case, we found that the results using a $(12\times12\times12)/(6\times6\times6)$ grid were already converged to 0.001 Å for the lattice constant of metals and to within all specified digits for C, Si, and MgO, justifying the coarser grids for the other insulating systems. We therefore consider the HSE03 calculations to be also fully converged with respect to the Brillouin sampling.

All PBE0 calculations were performed using $(12\times12\times12)/(12\times12\times12)$ k points, i.e., without downsampling. Admittedly, convergence is the slowest for the PBE0 functional and it is possible that errors are therefore somewhat larger for the PBE0 case than for the HSE03 and PBE cases. Unfortunately, our computational resources did not allow us to perform extensive convergence tests for the PBE0 case. Note that a downsampling is not possible for the PBE0 case, making calculations excessively demanding; see Sec. IV A.

B. FP-(L)APW+lo calculations

For further comparison, PBE calculations were performed for a selection of solids representing metals (Li, Al, Na, Cu, Rh, Pd, and Ag), semiconductors (GaAs), and insulators (MgO and C) using the full-potential (linearized) augmented plane wave [FP-(L)APW] plus local orbitals (lo) method as implemented in the WIEN2K code.[31] The APW+lo extension[32] was used for the valence electrons, since it allows for a faster convergence at the same high level of accuracy as the LAPW+lo approach. In order to enable a direct comparison of the FP-(L)APW+lo results with the PAW results, an identical k-point mesh for the Brillouin zone integration $(24\times24\times24)$ was used. In the WIEN2K program the accuracy is determined by the parameter $R_{MT}K_{max}$, i.e., the product of the smallest of the atomic muffin-tin radii R_{MT} in the system and the plane wave cutoff parameter, K_{max}. The R_{MT} and $R_{MT}K_{max}$ used in this work are summarized in Table III. Note that K_{max}^2 roughly corresponds to the energy cutoff in the PAW calculations (see Table I). Partial waves up to a momentum quantum number $l=10$ were used for the computation of the spherical matrix elements, whereas for the computation of the nonspherical matrix elements l was set to 4. The eigenvalues were calculated in an energy range between $E_{min}=-7.0$ Ry and $E_{max}=1.5$ Ry. Except in the case of Ag, E_{min} was reduced to −8.0 Ry, whereas for GaAs and C, E_{max} was increased to 2.0 and 2.5 Ry, respectively. For the latter three materials, the magnitude of the largest vector in the Fourier expansion of the charge density (G_{max}) was increased to 24 Ry and lm combinations, where m denotes the magnetic quantum number, up to an angular momentum of $l_{max}=8$, were included in the lattice harmonic expansion. For all other systems the default values ($G_{max}=14$ Ry and $l_{max}=6$) provided for these parameters were not changed.

IV. RESULTS AND DISCUSSION

A. Downsampling

The convergence of the total energy with respect to the k-mesh representation of the wave function and the q-mesh representation of the Fock exchange potential was investigated for all compounds in our set of materials. Two cases will be discussed in detail: Al (fcc) and MgO ($B1$). The conclusions drawn from Al are valid for the other metallic systems as well. MgO represents the insulating and semiconducting systems, which are much less demanding with respect to the Brillouin zone sampling.

Figure 1 shows the dependence of the total energy for fcc Al for all grid combinations listed in Table II. The upper panel presents the convergence behavior in the case of the HSE03 functional; the lower one gives the convergence behavior for the PBE0 functional. Figure 2 depicts the dependence of the Fock exchange energy for HSE03 and PBE0, respectively. Here, $n_{\mathbf{q}}$ is the number of q points for the Fock exchange along one of the symmetry equivalent directions; the sampling density in reciprocal space decreases from left to right in the plots. The zero of energy in Figs. 1 and 2 is taken to be the value for the $(24\times24\times24)/(24\times24\times24)$ k mesh (without downsampling).

The first important point is the convergence of the total energy with respect to the density of the k-point mesh, without downsampling of the Fock exchange interaction, $\{\mathbf{q}\}=\{\mathbf{k}\}$. These are usually the lowest energy points for each $n_{\mathbf{q}}$. Figure 1 shows the HSE03 total energy to be well converged using a $(12\times12\times12)$ mesh, whereas the energy difference between PBE0 calculations, employing $(12\times12\times12)$ and $(24\times24\times24)$ k points, still amounts to roughly 10 meV (note the different scales in both panels). A comparison to the corresponding data points in the lower panel of Fig. 2 shows this to be largely due to the change in the PBE0 Fock exchange energy.

The second relevant point is illustrated in Fig. 2, showing the convergence behavior of the HSE03 and PBE0 Fock exchange energies. The HSE03 Fock exchange energy is converged to 1 meV for a $(6\times6\times6)$ q-space mesh (circles connected by line), whereas the PBE0 Fock exchange energy still changes by roughly 5 meV from $(24\times24\times24)$ to $(12\times12\times12)$ q points and by almost 40 meV using a $(6\times6\times6)$ q mesh. The former is in good quantitative agreement with the arguments put forth in Sec. II B: for $\mu=0.3$ Å, R_{max}

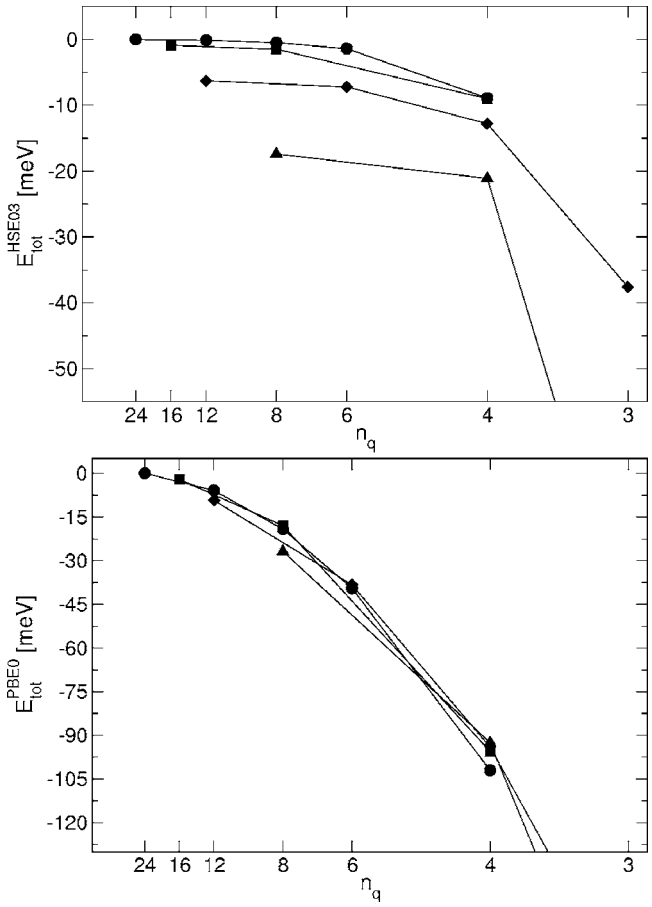

FIG. 1. Dependence of the total energy of fcc Al on the number of q points $n_{\mathbf{q}}$ (along one direction) used to sample the Fock exchange potential and on the size of the k-point grid used to represent the wave functions (triangles: $8\times8\times8$, diamonds: $12\times12\times12$, squares: $16\times16\times16$, and circles: $24\times24\times24$) (see Table II). HSE03 and PBE0 results are presented in the upper and lower panels, respectively.

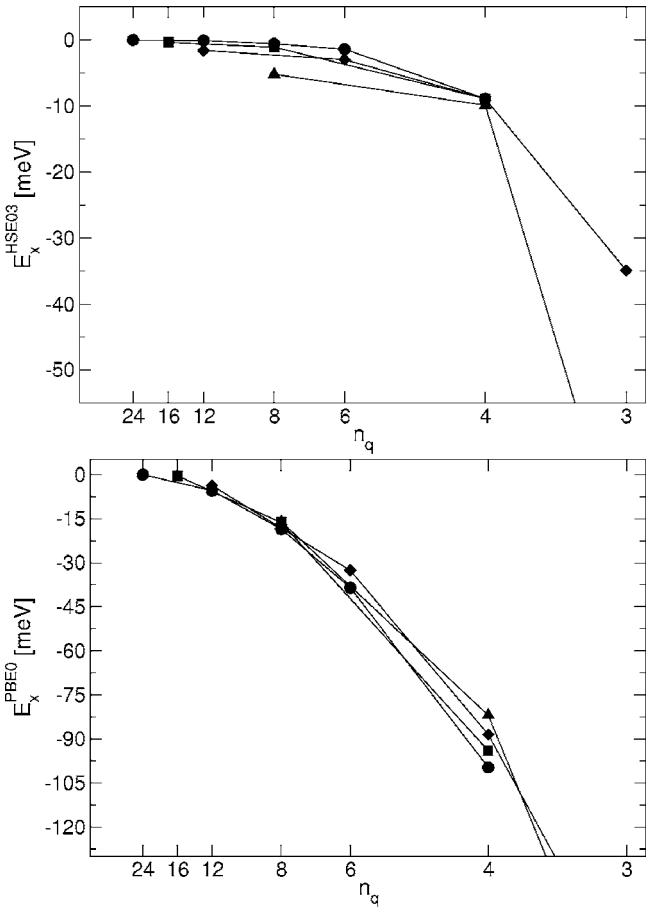

FIG. 2. Dependence of Fock exchange energy of fcc Al on the number of q points $n_{\mathbf{q}}$ (see Fig. 1 for details).

is 6.7 Å; the nearest-neighbor distance in Al is roughly 2.8 Å. With the condition $R_{\mathrm{NN}}>2R_{\max}$ (see Sec. II B), this leads to a maximally required $(5\times5\times5)$ sampling of the Fock exchange. Finally, we note that the error in the total energy is clearly dominated by the error in the Fock exchange energy for the PBE0 case and $(16\times16\times16)$ k points are required for well converged results.

Reasoning along these lines would lead us to the conclusion that in the case of MgO (nearest-neighbor distance ≈1.8 Å), one might need a $(8\times8\times8)$ mesh of q points to represent the short-range Fock exchange potential. However, as can be seen from Fig. 3, the typical situation in semiconducting and especially in insulating systems (MgO has a band gap of around 7.7 eV) is quite different to the situation in metallic systems. Insulating systems are much less demanding both with respect to the density of the overall k sampling of the BZ as well as with respect to the q-mesh representation of the Fock exchange interaction. The description of the HSE03 Fock exchange interaction is already sufficiently accurate using a $(4\times4\times4)$ mesh of q points and the PBE0 Fock exchange is shown to be converged on a $(12\times12\times12)$ mesh. This obviously results from the enhanced locality of the Wannier functions (see Sec. II B) in insulators, as compared with metallic systems.

B. Lattice parameters and bulk moduli

1. PBE calculations

Table IV lists the equilibrium lattice constants, a_0, and corresponding bulk moduli, B_0, for the considered test set of ionic, semiconducting, and metallic systems obtained using the PBE functional and the PAW method (this work), as well as the PBE results from Gaussian (GTO) local basis set cal-

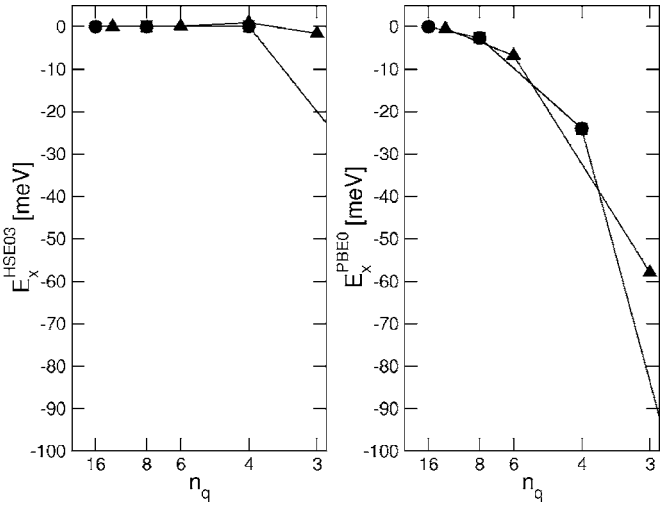

FIG. 3. Dependence of the Fock exchange energy of MgO on the number of q points $n_{\mathbf{q}}$ (see Fig. 1 for details). Left panel: HSE03; right panel: PBE0.

TABLE IV. Lattice constants, a_0 (Å), and bulk moduli, B_0 (GPa), obtained from PBE calculations. The results obtained using the PAW method are based on calculations employing a $(24\times24\times24)$ k-point grid. Column headings marked by a "‡" indicate GTO and experimental (Expt.) results taken from Ref. 8.

	PAW		GTO‡		Expt.‡	
Solid	a_0	B_0	a_0	B_0	a_0	B_0
Li	3.438	13.7	3.453	13.6	3.477	13.0
Na	4.200	7.80	4.199	7.7	4.225	7.5
Al	4.040	76.6	4.063	76.2	4.032	79.4
BN	3.626	370	3.629	368	3.616	400
BP	4.547	160	4.575	158	4.538	165
C	3.574	431	3.583	422	3.567	443
Si	5.469	87.8	5.490	88.6	5.430	99.2
SiC	4.380	210	4.401	207	4.358	225
β-GaN	4.546	169	4.539	183	4.520	210
GaP	5.506	75.3	5.493	80.4	5.451	88.7
GaAs	5.752	59.9	5.726	68.0	5.648	75.6
LiF	4.068	67.3	4.062	65.4	4.010	69.8
LiCl	5.150	31.5	5.148	32.7	5.106	35.4
NaF	4.707	44.6	4.700	47.3	4.609	51.4
NaCl	5.698	23.4	5.698	23.7	5.595	26.6
MgO	4.258	149	4.242	161	4.207	165
Cu	3.635	136	3.636	150	3.603	142
Rh	3.830	254	3.871	239	3.798	269
Pd	3.943	166	3.950	177	3.881	195
Ag	4.147	89.1	4.130	106	4.069	109
			All solids			
ME[a]	0.039	−12.3	0.042	−9.75	···	···
MAE[b]	0.045	12.4	0.047	10.6	···	···
rms[c]	0.054	16.4	0.054	14.5	···	···
			Without metals			
ME[a]	0.048	−13.4	0.049	−11.5	···	···
MAE[b]	0.048	13.4	0.049	11.5	···	···
rms[c]	0.059	17.2	0.056	14.9	···	···

[a]Mean error.
[b]Mean absolute error.
[c]Root mean square error.

culations (Ref. 8). The statistical data [mean error (ME), mean absolute error (MAE), and root mean square (rms) error] characterize the quality of the results in comparison to experiment.

First, we compare the PAW-PBE results with the experimental values. As usual, the PBE functional leads to an overestimation of the lattice constant, with the notable exceptions of Li and Na. The general agreement between the PBE lattice constants and experiment, however, is quite satisfactory; the largest relative error in the lattice constants amounts to 2.1%

TABLE V. Lattice constants, a_0 (Å), and bulk moduli, B_0 (GPa), obtained from PAW, FP-(L)APW+lo, and GTO calculations. The GTO results were taken from Ref. 8.

	PAW		FP-(L)APW+lo		GTO	
Solid	a_0	B_0	a_0	B_0	a_0	B_0
Li	3.438	13.7	3.436	13.8	3.453	13.6
Na	4.200	7.80	4.195	7.76	4.199	7.7
Al	4.040	76.6	4.041	76.3	4.063	76.2
C	3.574	431	3.573	430	3.583	422
MgO	4.258	149	4.258	149	4.242	161
GaAs	5.752	59.9	5.756	60.5	5.726	68.0
Cu	3.635	136	3.630	139	3.636	150
Rh	3.830	254	3.832	255	3.871	239
Pd	3.943	166	3.944	168	3.950	177
Ag	4.147	89.1	4.154	90.6	4.130	106

TABLE VI. Lattice constants, a_0 (Å), and bulk moduli, B_0 (GPa), obtained from HSE03 calculations using the PAW and local basis set (GTO) methods. Column headings marked by a "‡" indicate values taken from Ref. 8. $(24\times24\times24)/(8\times8\times8)$ k points were used for metals, C, Si, and MgO and $(12\times12\times12)/(12\times12\times12)$ k points were used for the remaining systems (see Sec. III A).

	PAW		GTO‡		Expt.‡	
Solid	a_0	B_0	a_0	B_0	a_0	B_0
Li	3.405	15.3	3.454	14.0	3.477	13.0
Na	4.162	8.74	4.166	9.9	4.225	7.5
Al	3.997	87.2	3.991	94.4	4.032	79.4
BN	3.593	407	3.603	398	3.616	400
BP	4.508	176	4.549	171	4.538	165
C	3.543	472	3.557	458	3.567	443
Si	5.419	100	5.454	99.1	5.430	99.2
SiC	4.338	234	4.370	225	4.358	225
β-GaN	4.489	198	4.498	207	4.520	210
GaP	5.450	87.3	5.455	91.4	5.451	88.7
GaAs	5.677	72.7	5.683	76.9	5.648	75.6
LiF	4.007	74.4	3.995	74.7	4.010	69.8
LiCl	5.097	34.2	5.098	36.3	5.106	35.4
NaF	4.638	50.4	4.631	52.2	4.609	51.4
NaCl	5.639	25.4	5.638	25.7	5.595	26.6
MgO	4.201	172	4.200	175	4.207	165
Cu	3.630	129	3.631	143	3.603	142
Rh	3.779	291	3.838	262	3.798	269
Pd	3.910	170	3.932	181	3.881	195
Ag	4.137	87.7	4.129	104	4.069	109
			All solids			
ME[a]	−0.006	1.2	0.007	1.5	···	···
MAE[b]	0.029	9.1	0.026	4.7	···	···
rms[c]	0.035	12.5	0.031	6.8	···	···
			Without metals			
ME[a]	−0.004	3.8	0.006	2.7	···	···
MAE[b]	0.020	6.9	0.017	3.7	···	···
rms[c]	0.024	10.2	0.021	5.6	···	···

[a]Mean error.
[b]Mean absolute error.
[c]Root mean square error.

(for NaF) and the ME and MAE to 0.039 and 0.045 Å, respectively. Disregarding the metallic systems slightly worsens this picture. We note that the experimental lattice constants in Table IV were not corrected for the anharmonic expansion arising from zero-point vibrations. Since anharmonicity corrections yield slightly smaller experimental lattice constants,[33] a small increase of the ME and MAE in the lattice constant is expected.

As is obvious from Table IV the overestimation of the lattice constant shows a one-to-one correlation with an underestimation of the bulk modulus. Since the calculated bulk moduli are quite sensitive to the equilibrium volume at which they are evaluated, an error in the theoretical lattice constant with respect to experiment translates into a comparatively large discrepancy in B_0. This is clearly born out by the ME and MAE of the PAW-PBE bulk moduli with respect to experiment, which amount to −12.3 and 12.4 GPa, respectively.

The second point concerns the comparison between our PAW-PBE results and the GTO results of Ref. 8. As can be seen from Table IV, the overall agreement between the PAW- and GTO-PBE results is good; e.g., the mean deviation and mean absolute deviation of the PAW-PBE lattice constants, with respect to their GTO counterparts, are 0.004 and 0.013 Å, respectively, and the PAW and the GTO results show similar ME and MAE with respect to experiment. Nonetheless, in some cases the discrepancies are noteworthy: (i) for several systems the difference between the PAW and GTO lattice constants is relatively large (Li, Al, C, Si, SiC, GaAs, Rh, and Ag) and (ii) for several systems the GTO bulk modulus is significantly higher than its PAW counterpart, although the corresponding GTO lattice constant is *larger* than (or roughly equal to) the PAW lattice constant (Li, Si, Cu, and Pd).

These discrepancies can be attributed to either the differences in the basis sets (projector augmented plane waves versus contracted Gaussian orbitals), or to the quality of the PAW description of the interaction between the valence electrons and the ionic cores, or to both. As an independent benchmark we performed FP-(L)APW+lo calculations (see Sec. III B) on Li, Na, Al, C, MgO, GaAs, Cu, Rh, Pd, and

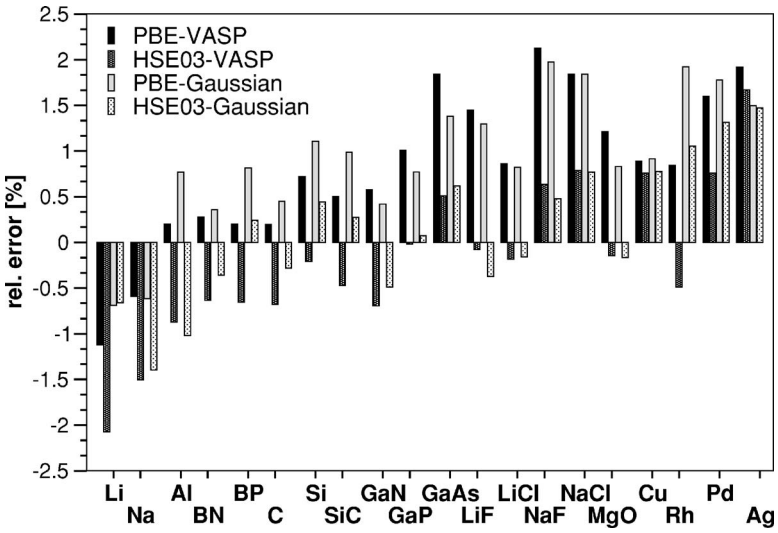

FIG. 4. Relative errors of the lattice constants with respect to experiment for PBE and HSE03 using plane waves and GTOs (Ref. 8).

Ag. The results are listed in Table V. As can be clearly seen, the agreement between the PAW and FP-(L)APW+lo calculations is excellent (they are *de facto* identical), both for the lattice constants as well as for the bulk moduli.

The most probable explanation for the discrepancies between the PAW and GTO results, therefore, is that the Gaussian basis sets used in Ref. 8 were not yet fully converged at least for some of the systems listed in Table IV, especially for the prediction of bulk moduli in *d* metals. We note that a recent publication of Heyd *et al.*[9] gives slightly different lattice constants (without bulk moduli). For C, MgO, and GaAs they reported values of 3.579, 4.268, and 5.771 Å, respectively, which are somewhat larger than the plane wave results.[8] Obviously, convergence is difficult to attain using GTOs. This is an important point to keep in mind as we turn to the discussion of the PAW- and GTO-HSE03 results, since basis set errors at the PBE level will carry over to the related hybrid functionals.

2. HSE03 calculations

Table VI lists the PAW and GTO (from Ref. 8) lattice constants and bulk moduli obtained using the HSE03 functional. Again the experimental data are shown as well to ease comparison. The HSE03 results are in better agreement with the experiment than those obtained using the PBE functional (see Table IV). The ME and MAE in the HSE03 lattice constants and bulk moduli amount to −0.006 Å, 0.029 Å, 1.2 GPa, and 9.1 GPa, respectively, compared with 0.039 Å, 0.045 Å, −12.3 GPa, and 12.4 GPa, for the PBE calculations. On average the HSE03 lattice constants are contracted by ≈1% with respect to their PBE counterparts (largest contractions: ≈1.5% for LiF and NaF). Whereas the PBE results show an almost consistent overestimation with respect to experiment, the HSE03 functional leads to an underestimation of the equilibrium volume in most cases (see Tables IV and VI). Unsurprisingly, the contraction of the HSE03 lattice parameter with respect to the PBE results goes hand in hand with an increase in the bulk moduli by roughly 10% (with the exceptions of Cu and Ag). Figures 4 and 5 provide a graphical representation of the aforementioned trends both for our PAW calculations as well as for the GTO results of Ref. 8.

As can be clearly seen from Fig. 4, the GTO-HSE03 lattice constants of Heyd and Scuseria[8] show the same general trend as our PAW calculations, although somewhat less pronounced (an average contraction of the lattice constant of

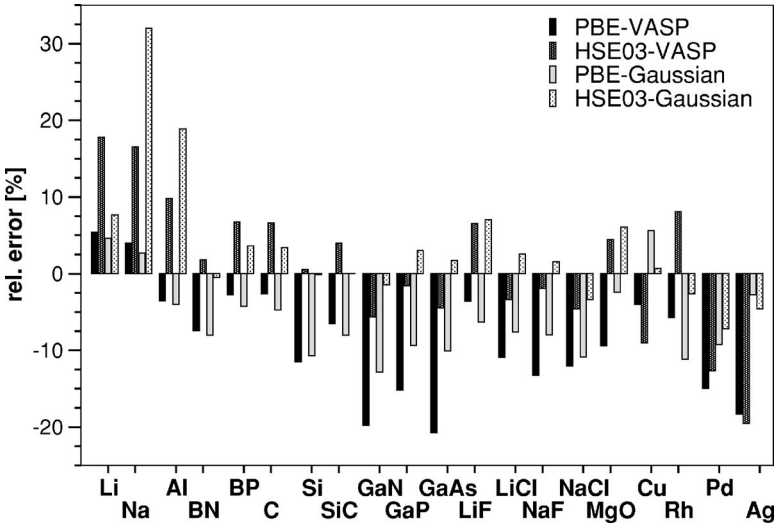

FIG. 5. Relative errors of the bulk modulus constants with respect to experiment for PBE and HSE03 using plane waves and GTOs (Ref. 8).

0.8%) and in some cases a bit erratic (e.g., Li shows a slight expansion of the lattice constant). Whereas the PAW-HSE03 lattice constants underestimate the experimental values, the GTO-HSE03 lattice constants on average still slightly overestimate the lattice constants, although the respective MEs and MAEs are of comparable magnitude (see Table VI). Inclusion of zero-point vibration effects would improve the agreement of the PAW results with experiment.

The same holds for bulk moduli, where an increase is observed from PBE to HSE03, both for the plane waves and for local basis sets (Fig. 5). Intriguingly, a lowering of the Cu and Ag bulk moduli at *smaller* lattice constant in comparison to PBE is shown by both the GTO and PAW calculations. However, as can be seen from the MAEs in Table VI, the GTO-HSE03 calculations seemed to perform much better with respect to experiment than the corresponding PAW calculations (4.7 versus 9.1 GPa). We believe this to be due to a fortuitous cancellation of basis set errors in the case of the GTOs. The differences stem mainly from the results for C, SiC, GaAs, and the *d*-metal systems (Cu, Rh, Pd, and Ag), for which we have already demonstrated that the local basis set calculations do not match our PAW and FP-(L)APW +lo results on the PBE level.

3. PBE0 calculations

Table VII lists the lattice constants and bulk moduli obtained from PBE0 calculations and the corresponding data from experiment. Comparing the statistical data listed in Tables VI and VII, it is clear that the PBE0 results present a further slight improvement over the HSE03 functional. On average the PBE0 lattice constants show a slight expansion of ≈0.3% in comparison to the corresponding HSE03 results and the bulk moduli are typically reduced by about 1%–2%, with the exception of GaN, GaAs, Cu, Rh, and Pd.

The relatively modest improvement of the PBE0 calculation in comparison to the HSE03 functional has to be weighed against the computational advantages of the HSE03 functional. We suppose that the latter outweighs the moderate improvements in the quality of results.

C. Atomization energies and heats of formation

Table VIII lists the atomization energies as obtained from PBE, PBE0, and HSE03 calculations. The atomization energy, $\varepsilon_0(M)$, of a material M, with N atoms in the unit cell, is defined as

$$\varepsilon_0(M) = \frac{1}{N}\left\{ \sum_{\text{atoms}} E_0(X) - E_0(M) \right\}, \tag{17}$$

where $E_0(M)$ is the total energy of the bulk system and $E_0(X)$ the corresponding energy of the constituent atoms, X at standard pressure. All energies in Table VIII are given in eV/atom and the ME, MAE, and mean absolute relative error (MARE) are calculated with respect to the experimental data of Ref. 34 (listed as well). Note that our calculated atomization energies are not corrected for zero-point vibrational contributions, which would lower the theoretical atomization energies. This should be taken into consideration when comparing the calculations presented here with the results of Ref. 33. Experimental values are based on zero-temperature enthalpies of formation ($\Delta_f H_0^o$) of the crystals and gaseous atoms.[34] As Table VIII clearly shows, the overall description of the atomization energies of our set of systems is best at the PBE level, with a MARE of 3.4%, compared with 7.6% and 6.7% for the PBE0 and HSE03 results, respectively. A comparison between the ME, MAE, and MARE listed in Table VIII for the complete set of systems and the corresponding entries for the nonmetallic systems only shows that the PBE0 and HSE03 hybrids underperform with respect to the PBE functional, especially for *d* metals. For the subset of nonmetallic systems, the ME, MAE, and MARE in the PBE, PBE0, and HSE03 cases are quite comparable, at least within the error margin introduced by the neglect of zero-point vibrational energies. The main reason for the large reduction of the atomization energy of *d* metals is related to the increased stability of the spin-polarized atom compared with an artificial non-spin-polarized atom. Most likely, the hybrid functionals overestimate the exchange splitting in *d* elements, with a concomitant increase of the spin-polarization energy. We will see a related error for bcc Fe in the next section.

TABLE VII. Lattice constants, a_0 (Å), and bulk moduli, B_0 (GPa), obtained from PBE0 calculations using the PAW method. Experimental data were taken from Ref. 8. For all systems, a $(12\times12\times12)/(12\times12\times12)$ k-point grid was used (see Sec. III A).

	PAW		Expt.	
Solid	a_0	B_0	a_0	B_0
Li	3.463	13.7	3.477	13.0
Na	4.229	8.22	4.225	7.5
Al	4.012	86.0	4.032	79.4
BN	3.600	402	3.616	400
BP	4.520	174	4.538	165
C	3.549	467	3.567	443
Si	5.433	99.0	5.430	99.2
SiC	4.347	231	4.358	225
β-GaN	4.481	199	4.520	210
GaP	5.446	87.3	5.451	88.7
GaAs	5.682	72.7	5.648	75.6
LiF	4.011	72.8	4.010	69.8
LiCl	5.110	33.5	5.106	35.4
NaF	4.648	48.7	4.609	51.4
NaCl	5.654	24.6	5.595	26.6
MgO	4.211	169	4.207	165
Cu	3.636	130	3.603	142
Rh	3.785	291	3.798	269
Pd	3.915	172	3.881	195
Ag	4.142	86.8	4.069	109
	All solids			
ME[a]	0.007	−0.1	···	···
MAE[b]	0.022	7.9	···	···
rms[c]	0.029	11.3	···	···
	Without metals			
ME[a]	0.003	1.9	···	···
MAE[b]	0.019	5.4	···	···
rms[c]	0.026	8.2	···	···

[a]Mean error.
[b]Mean absolute error.
[c]Root mean square error.

TABLE VIII. Atomization energies obtained from PBE, PBE0, and HSE03 calculations. Note that the energy values are not corrected for zero-temperature vibration effects. All energies are given in eV/atom.

Solid	PBE	PBE0	HSE03	Expt.
Li	1.605	1.516	1.577	1.63
Na	1.079	0.985	1.028	1.13
Al	3.434	3.385	3.492	3.39
BN	6.928	6.811	6.796	6.68
BP	5.287	5.247	5.232	5.04
C	7.706	7.592	7.565	7.37
Si	4.556	4.555	4.553	4.63
SiC	6.403	6.387	6.387	6.34
β-GaN	4.389	4.371	4.281	4.48
GaP	3.484	3.542	3.466	3.56
GaAs	3.151	3.125	3.109	3.26
LiF	4.327	4.215	4.303	4.40
LiCl	3.358	3.347	3.408	3.55
NaF	3.824	3.690	3.782	3.90
NaCl	3.087	3.069	3.136	3.31
MgO	5.013	4.924	5.014	5.15
Cu	3.484	3.046	3.088	3.49
Rh	5.724	4.205	4.344	5.75
Pd	3.706	2.882	2.998	3.89
Ag	2.518	2.329	2.373	2.95
		All solids		
ME[a]	−0.042	−0.234	−0.198	···
MAE[b]	0.136	0.295	0.264	···
MARE[c]	3.4	7.6	6.7	···

[a]Mean error.
[b]Mean absolute error.
[c]Mean absolute relative error (%).

Because of the increased discrepancies to experiment, which are mainly related to problems in atoms, one might hope for improved results for the heat of formation, ΔH_f, a key quantity in thermochemistry. For the elementary reaction

$$A(s) + \tfrac{1}{2}B_2(g) \rightarrow AB(s), \tag{18}$$

it is defined as

$$\Delta H_f[AB(s)] = E_{\mathrm{tot}}[AB(s)] - \left(E_{\mathrm{tot}}[A(s)] + \tfrac{1}{2}E_{\mathrm{tot}}[B_2(g)]\right), \tag{19}$$

where s and g refer to a compound in the solid and gas phases, respectively. Table IX lists the PBE, PBE0, and HSE03 values for several reactions covered by the test set. For the molecules involved in the gas-phase reactions, "harder" PAW potentials instead of those given in Table I were utilized (see Ref. 11). To correct for the resulting error, the energy difference between the spherical atoms calculated with the standard and the hard PAW data set was added. This correction, however, changes the results only little, leading to a mean error of around 0.5%. Whereas the PBE results show a pronounced underestimation for the heat of formation (14% with respect to experiment), the PBE0 and especially the HSE03 hybrid functional perform markedly better, with MAREs of 9% and 6%, respectively. Although the set of systems listed in Table IX cannot be termed representative, these results are encouraging and relativize the large discrepancies for the atomization energies at the PBE0 and HSE03 levels.

TABLE IX. The theoretical heats of formation for six insulators obtained by the application of the PBE, PBE0, and HSE03 functionals. The theoretical and experimental values are for $T=0$ K; the theoretical ones are not corrected for zero-point vibration effects. The data are given in kJ/mol.

Solid	PBE	PBE0	HSE03	Expt.[c]
LiF	−568.5	−592.3	−605.4	−614
LiCl	−356.2	−374.1	−382.9	−408
NaF	−522.1	−542.2	−558.0	−573
NaCl	−354.7	−371.9	−383.6	−411
MgO	−521.2	−543.5	−554.8	−597
SiC	−52.4	−60.2	−63.0	−71
ME[a]	49.8	31.7	21.0	···
MARE[b]	13.6	8.5	6.3	···

[a]Mean error.
[b]Mean absolute relative error (%).
[c]Ref. 34.

D. Band gaps and magnetic properties

In order to investigate the performance of hybrid functionals applied to the calculations of electronic properties, we present results for GaAs (zinc blende), Si (cubic diamond), C (cubic diamond), MgO ($B1$), NaCl ($B1$), and Ar (fcc) band gaps. The data given in Table X show the differences between the eigenvalues of the highest occupied band at the Γ point and the lowest unoccupied band at the Γ, X, and L points, except for Ar, for which we report only the Γ-Γ gap. These calculations applying the PBE, PBE0, and HSE03 functionals have been carried out at the experimental lattice constant.

As usual, the DFT (PBE) calculations show the typical underestimation of band gaps. Generally one can conclude that admixing Fock exchange definitely improves the gaps upon the pure DFT calculations. For the HSE03 case, the improvements are most notable for systems with a small to medium gap size, whereas for large-gap systems, such as NaCl and Ar, the band gaps are still underestimated. The PBE0 functional overestimates the band gaps for semiconductors and still underestimates it for large-gap insulators; the PBE0 results are almost uniformly shifted by 0.8 eV with respect to the HSE03 values.

The failure for large-gap systems can be understood by realizing the analogies between simple model GW approaches (static COH-SEX) and hybrid functionals.[44] We note that GW gives an excellent account of band gaps for semiconductors and insulators.[45] In both cases, a fraction of the nonlocal exchange is experienced by the electrons, but in the GW method its amount is determined by multiplying the bare nonlocal exchange operator with the inverse of the dielectric function. Hence, in large-gap systems, where screening is very weak, the nonlocal exchange term should approach the bare Fock exchange, whereas for systems with an intermediate screening (medium gap size), the HSE03 functional has just the right balance.

For metals, we also find that the results using the hybrid functionals are not entirely satisfactory. In general the

TABLE X. Direct and indirect gaps (eV) for GaAs, Si, C, MgO, NaCl, and Ar for the Γ, X, and L points using the PBE, PBE0, and HSE03 functionals.

	PBE	PBE0	HSE03	Expt.
		GaAs		
$\Gamma_{15v}\rightarrow\Gamma_{1c}$	0.56	2.01	1.29	1.52[a]
$\Gamma_{15v}\rightarrow X_{1c}$	1.46	2.67	1.99	1.90[a]
$\Gamma_{15v}\rightarrow L_{1c}$	1.02	2.37	1.64	1.74[a]
		Si		
$\Gamma'_{25v}\rightarrow\Gamma_{15c}$	2.57	3.97	3.19	3.34–3.36,[b] 3.05[c]
$\Gamma'_{25v}\rightarrow X_{1c}$	0.71	1.93	1.23	1.13,[d] 1.25[c]
$\Gamma'_{25v}\rightarrow L_{1c}$	1.54	2.88	2.13	2.06(3),[e] 2.40(15)[f]
		C		
$\Gamma'_{25v}\rightarrow\Gamma_{15}$	5.59	7.69	6.77	7.3[a]
$\Gamma'_{25v}\rightarrow X_{1c}$	4.76	6.66	5.76	
$\Gamma'_{25v}\rightarrow L_{1c}$	8.46	10.77	9.80	
		MgO		
$\Gamma_{15}\rightarrow\Gamma_1$	4.75	7.24	6.34	7.7[g]
$X_{4'}\rightarrow\Gamma_1$	9.15	11.67	10.79	
$L_1\rightarrow\Gamma_1$	7.91	10.38	9.49	
		NaCl		
$\Gamma_{15}\rightarrow\Gamma_1$	5.20	7.26	6.45	8.5[h]
$X_{4'}\rightarrow\Gamma_1$	7.60	9.66	8.78	
$L_1\rightarrow\Gamma_1$	7.32	9.41	8.57	
		Ar		
$\Gamma_{15}\rightarrow\Gamma_1$	8.68	11.09	10.25	14.2[i]

[a]Reference 35.
[b]Reference 36.
[c]Reference 37.
[d]References 36 and 38.
[e]Reference 39.
[f]Reference 40.
[g]Reference 41.
[h]Reference 42.
[i]Reference 43.

HSE03 functional increases the bandwidth. The Na valence bandwidth, for instance, increases from 3.3 to 3.7 eV (4.3 eV) using the HSE03 (PBE0) functional and for Al it increases from 11.1 to 12.5 eV (13.1 eV). The experimental x-ray photoemission spectroscopy (XPS) spectra are reproduced accurately using the LDA densities of states,[46] which suggests that the HSE03 bandwidths are slightly and the PBE0 bandwidths significantly too large. In particular, for Al the XPS spectrum shows the onset of the valence band well above 12 eV ($\approx$12.5 eV).[46]

More severe problems are encountered for itinerant magnetic systems. We have performed only a few tests for Fe, Co, and Ni and concentrate on the Fe case here, expecting these observations to carry over to other itinerant magnetic systems. For Fe, the magnetic moment is $2.2\mu_B$ using the PBE functional, in excellent agreement with experiment ($2.2\mu_B$).[25] Using the HSE03 functional, the magnetic moment increases to $2.7\mu_B$ and the exchange splitting is significantly overestimated compared with experiment. Considering the previous analogy between *GW* and hybrid functionals, failures for metals are not unexpected. In the strongly screening metals, the inverse dielectric function approaches zero and hence the nonlocal exchange term in the *GW* approximation is strongly screened. Using 25% of the nonlocal exchange term thus leads to an overestimation of the exchange splitting and bandwidth in metals.

V. CONCLUSIONS

In this work, the performance of screened hybrid density functionals, in particular, the HSE03 and PBE0 functionals, was rigorously assessed through calculations of structural (equilibrium lattice constants, bulk moduli), thermochemical (cohesive energies, heats of formation), and electronic properties (band gaps) of semiconductors and insulators. For this purpose, a representative test set of 20 materials comprising ionic, semiconducting, and metallic systems was chosen. The implementation of hybrid functionals, which requires inclusion of a fraction of the nonlocal Fock exchange, was done in a plane wave based code using the PAW method. This allows for basis-set-superposition-free calculations and one can benefit from computationally efficient fast Fourier transforms.

The obtained results have been compared first with experimental values and second to literature results based on calculations using Gaussian-type orbitals (GTOs). In general, the discrepancies between PAW and the GTO calculations are moderate but still not entirely negligible. We believe that the PAW results are more reliable, as demonstrated by additional FP-(L)APW+lo calculations on the PBE level, which gave *de facto* identical properties as the PAW method.

Our main findings still agree with the previous assessment based on GTOs.[8] The equilibrium lattice constants decrease using the hybrid functionals, bringing them in better agreement with experiment. Also the bulk moduli are improved. It is, however, still too early to use the hybrid functionals routinely as a replacement for the traditional semilocal functionals, as demonstrated by the results for transition metals. The cohesive energy of these systems is significantly underestimated, which can be traced back to an overestimated exchange splitting and spinpolarization energy in *d* elements. This also leads to an overestimation of the predicted magnetic moment in bcc Fe and other 3*d* metals.

If these special cases are excluded, we find that the atomization energies of the considered solids agree well with experiment. The results of thermochemical calculations are even more promising insofar that the HSE03 functional yields heats of formation that are improved compared with both the semilocal PBE functional as well as the hybrid PBE0 functional. Band gaps are also clearly improved by admixing a fraction of the bare Fock exchange, although we again find the improvement to be nonuniversal. For large-gap systems the HSE03 functional still seriously underestimates the band gaps, whereas for metals the bandwidth seems to be slightly overestimated. Using the analogy between *GW* and hybrid functionals it is argued that more of the exact exchange would be required in large-gap systems and less in metals or strongly screening materials. It might well be that this is also the main reason why the exchange splitting is overestimated in *d* elements, where the long-range exchange contribution is efficiently screened by the *s* and *p* electrons and by screening between open-shell *d* orbitals (near degeneracy of multiplets in atoms).

Finally we want to comment on the computational performance of hybrid functionals in solids. We find that only a few k points are required to calculate the nonlocal exchange energy (and total energy) in the case of the HSE03 functional. This favorable behavior is related to the fact that only the short-range Fock exchange is included in the HSE03 functional. One can exploit this behavior in periodic codes by restricting the k-point mesh in the evaluation of the nonlocal exchange operator. Typically we find that $(6\times6\times6)$ k points are more than sufficient to accurately represent the screened exchange interaction even in metals, whereas at least $(12\times12\times12)$ k points are required if the bare (unscreened) exchange operator is used. As for real space codes, the HSE03 functional is therefore clearly preferable than the PBE0 functional, where the overall convergence is dominated by the Fock exchange.

ACKNOWLEDGMENTS

The authors acknowledge Dr. J. Heyd for providing us some technical details concerning the HSE03 functional. This work was supported by the Austrian *Fonds zur Förderung der wissenschaftlichen Forschung* within the START grant.

[1] J. P. Perdew and K. Schmidt, in *Density Functional Theory and its Applications to Materials*, edited by V. van Doren, C. van Alsenoy, and P. Geerlings (AIP, Melville, NY, 2001).
[2] J. P. Perdew, Phys. Rev. Lett. **55**, 1665 (1985).
[3] A. D. Becke, J. Chem. Phys. **98**, 1372 (1993).
[4] J. P. Perdew, M. Ernzerhof, and K. Burke, J. Chem. Phys. **105**, 9982 (1996).
[5] J. Muscat, A. Wander, and N. M. Harrison, Chem. Phys. Lett. **342**, 397 (2001).
[6] T. Bredow and A. R. Gerson, Phys. Rev. B **61**, 5194 (2000).
[7] J. Heyd, G. E. Scuseria, and M. Ernzerhof, J. Chem. Phys. **118**, 8207 (2003).
[8] J. Heyd and G. E. Scuseria, J. Chem. Phys. **121**, 1187 (2004).
[9] J. Heyd, J. E. Peralta, G. E. Scuseria, and R. L. Martin, J. Chem. Phys. **123**, 174101 (2005).
[10] J. Tao, J. P. Perdew, V. N. Staroverov, and G. E. Scuseria, Phys. Rev. Lett. **91**, 146401 (2003).
[11] J. Paier, R. Hirschl, M. Marsman, and G. Kresse, J. Chem. Phys. **122**, 234102 (2005).
[12] G. Kresse and J. Hafner, Phys. Rev. B **48**, 13115 (1993).
[13] G. Kresse and J. Furthmüller, Comput. Mater. Sci. **6**, 15 (1996); Phys. Rev. B **54**, 11169 (1996).
[14] F. Gygi and A. Baldereschi, Phys. Rev. B **34**, 4405 (1986).
[15] C. Adamo and V. Barone, J. Chem. Phys. **110**, 6158 (1999).
[16] J. P. Perdew, K. Burke, and M. Ernzerhof, Phys. Rev. Lett. **77**, 3865 (1996).
[17] M. Ernzerhof, Chem. Phys. Lett. **263**, 499 (1996).
[18] V. N. Staroverov, G. E. Scuseria, J. Tao, and J. P. Perdew, J. Chem. Phys. **119**, 12129 (2003).
[19] J. Jaramillo, G. E. Scuseria, and M. Ernzerhof, J. Chem. Phys. **118**, 1068 (2003).
[20] R. D. Adamson, J. P. Dombroski, and P. M. W. Gill, Chem. Phys. Lett. **254**, 329 (1996).
[21] P. M. W. Gill and R. D. Adamson, Chem. Phys. Lett. **261**, 105 (1996).
[22] A. Savin, in *Recent Developments and Applications of Modern Density Functional Theory*, edited by J. M. Seminario (Elsevier, Amsterdam, 1996), p. 327.
[23] T. Leininger, H. Stoll, H.-J. Werner, and A. Savin, Chem. Phys. Lett. **275**, 151 (1997).
[24] P. E. Blöchl, Phys. Rev. B **50**, 17953 (1994).
[25] G. Kresse and D. Joubert, Phys. Rev. B **59**, 1758 (1999).
[26] J. G. Ángyán, I. C. Gerber, and M. Marsman (unpublished).
[27] G. Kresse and J. Hafner, J. Phys.: Condens. Matter **6**, 8245 (1994).
[28] F. D. Murnaghan, Proc. Natl. Acad. Sci. U.S.A. **30**, 244 (1944).
[29] H. J. Monkhorst and J. D. Pack, Phys. Rev. B **13**, 5188 (1976).
[30] P. E. Blöchl, O. Jepsen, and O. K. Andersen, Phys. Rev. B **49**, 16223 (1994).
[31] P. Blaha, K. Schwarz, G. K. H. Madsen, D. Kvasnicka, and J. Luitz, WIEN2K, an augmented plane wave+local orbitals program for calculating crystal properties, Vienna University of Technology, Vienna, 2001, ISBN 3-9501031-1-2.
[32] E. Sjöstedt, L. Nordström, and D. J. Singh, Solid State Commun. **114**, 15 (2000).
[33] V. N. Staroverov, G. E. Scuseria, J. Tao, and J. P. Perdew, Phys. Rev. B **69**, 075102 (2004).
[34] *NIST-JANAF Thermochemical Tables*, edited by M. W. Chase, Jr. (AIP, New York, 1998).
[35] *Numerical Data and Functional Relationships in Science and Technology*, Landolt-Börnstein, New Series, Group III, Vols. 17 and 22, Pt. A, edited by K.-H. Hellwege, O. Madelung, M. Schulz, and H. Weiss (Springer-Verlag, New York, 1982).
[36] M. Walkowsky and R. Braunstein, Phys. Rev. B **5**, 497 (1972).
[37] J. E. Ortega and F. J. Himpsel, Phys. Rev. B **47**, 2130 (1993).
[38] R. R. Zucca, J. P. Walter, Y. R. Shen, and M. L. Cohen, Solid State Commun. **8**, 627 (1970).
[39] R. Hulthén and N. G. Nilsson, Solid State Commun. **18**, 1341 (1976).
[40] D. Straub, L. Ley, and F. J. Himpsel, Phys. Rev. Lett. **54**, 142 (1985).
[41] S. Adachi, *Optical Properties of Crystalline and Amorphous Semiconductors: Numerical Data and Graphical Information* (Kluwer Academic, Dordrecht, 1999).
[42] R. T. Poole, J. Liesegang, R. C. G. Leckey, and J. G. Jenkin, Phys. Rev. B **11**, 5190 (1975).
[43] R. J. Magyar, A. Fleszar, and E. K. U. Gross, Phys. Rev. B **69**, 045111 (2004).
[44] S. Massidda, M. Posternak, and A. Baldereschi, Phys. Rev. B **48**, 5058 (1993).
[45] F. Aryasetiawan and O. Gunnarsson, Rep. Prog. Phys. **61**, 237 (1998).
[46] *Photoemission in Solids II, Case studies*, Topics in Applied Physics Vol. 27, edited by L. Ley and M. Cardona (Springer, New York, 1979).